Uncooled micromachined bolometer arrays on flexible substrates

Shadi A. Dayeh, Donald P. Butler,* Zeynep Çelik-Butler
University of Texas at Arlington, Electrical Engineering Department
P.O. Box 19072, Arlington, Texas, 76019
and
Patty Wisian-Neilson
Southern Methodist University, Chemistry Department
P.O. Box 750314 Dallas, TX 75275

ABSTRACT

This paper reports progress on the development of micromachined infrared microsensors on flexible polymer substrates. The flexible substrates were formed by spin-coating polyimide films (HD Microsystems PI-5878G) on silicon wafer carriers. Semiconducting Yttrium Barium Copper Oxide (YBCO) was used as the thermistor. The microbolometer was fabricated using a polyimide (HD Microsystems PI2737) sacrificial mesa and titanium electrode arms. The YBCO thermistor was suspended above the substrate by the electrode arms after the sacrificial layers have been removed by micromachining. The polyimide substrate was then removed from the silicon wafer carrier to complete the fabrication of the infrared microsensors on a flexible polyimide substrate. The measured thermal conductance of the microbolometers ranged from 9.07×10^{-6}W/K for a non-micromachined to 4.0×10^{-7}W/K for a micromachined sensor. As a result, the responsivity and detectivity were measured to be as high as 6.1×10^{4}V/W and a 1.2×10^{8} cmHz$^{1/2}$/W, respectively, with a 970 nA current bias. This level of performance is comparable to similar micromachined detectors fabricated on silicon substrates.

Keywords: Microbolometers, flexible substrate, micromachining, yttrium barium copper oxide, MEMS, Smart Skin.

1. INTRODUCTION

Flexible microsensors are attracting considerable attention due to their potential applications in robotics and their ability to conform to non-planar surfaces. Flexible microsensors have the potential to be integrated with Si thin-film transistors [1] or polymer transistors [2] to provide electronic read out circuitry to achieve a smart sensitive skin. The interest in flexible microsensors is stimulated by their light weight, mechanical flexibility, potential for low cost, enabling artificial sensitive skin, and the potential for integration with clothing. Other efforts to make flexible MEMS microsensors include the development of shear stress sensors on Si islands connected by flexible polyimide films to form a flexible skin [3,4]. These devices however did not eliminate the use of rigid silicon. The same technology was investigated in 1994, however the silicon suffered from breakage at the island periphery [5]. Heat flux sensors have been formed by direct deposition of metal films on commercial Kapton [6]. Our previous investigation of infrared (IR) microsensors on Kapton substrates includes bonding Kapton sheets to silicon wafer carriers. This technique suffered from trapped air bubbles between the silicon and the Kapton film as well as from thermal expansion of the Kapton film during fabrication [7]. Spin-coating a silicon wafer with polyimide [8] was also successfully used to fabricate microbolometers, however in both cases, the microbolometers were not micromachined, but were fabricated directly on the polyimide (Kapton) surface. Micromachining reduces the sensor's energy loss due to thermal conduction and reduces the sensor's thermal mass to improve the microbolometer performance.

In this work, we have improved the performance of the previous infrared microsensors on flexible substrates [7,8] by using a micromachined bridge structure. This has increased the performance of the microbolometers to be comparable to identical micromachined microbolometers previously fabricated using Si substrates. Previously, surface and bulk micromachining was applied to fabricate infrared sensors on silicon substrates using three different techniques:

* Author of correspondence: dbutler@uta.edu

Downloaded From: http://proceedings.spiedigitallibrary.org/ on 06/04/2013 Terms of Use: http://spiedl.org/terms

(1) etching into silicon itself [9,10]; (2) using an MgO sacrificial layer [11]; and (3) using a polyimide sacrificial layer [12]. For this work, a high temperature polyimide coating [13], HD Microsystems PI-5878G, was used as the flexible substrate. PI-5878G is a high molecular weight, polyamic acid; precursor in an NMP [N-methyl-2-pyrrolidoline] based solvent system. After being applied to a substrate such as silicon, the precursor was thermally converted into an intractable polyimide film. After the devices have been fabricated, the carrier silicon wafer was diced into small die and the flexible polyimide was removed, producing micromachined structures on a flexible substrate. The properties of PI-5878G are similar to Kapton, a relatively well-known material used as a flexible substrate. The properties of PI-5878G and other flexible substrate materials are compared to silicon in Table I. In contrast to silicon, polymer substrates require low temperature processing and possess lower tensile strength and tensile modulus than silicon. However, polymer substrates have greater flexibility and have potential for low cost, large area electronic applications.

Table I. Typical room temperature properties for commercially available flexible substrates compared to silicon.

Material	*Commercial Name (Manufact.)*	*Tensile Modulus (psi)*	*Tensile Strength (psi)*	*Max. Temp. (°C)*	*Coeff. Of Linear Thermal Expansion (m/m/°C) (-18 – 150 °C)*	*Volume Resistivity Ohm - cm*	*Chemical Resistance*
PEI Polyetherimid	Ultem (GE)	$4.8x10^5$ – $1.3x10^6$	$1.4x10^4$ – $2.8x10^4$	190 - 215	$5.5x10^{-5}$	$1.0x10^{17}$	Fair to good
PEEK Polyetherether ketone	Victrex (ICI) Thermocomp (LNP)	$4.4x10^5$ – $2.4x10^6$	$1.4x10^4$ – $4.1x10^4$	250 - 315	1.8 – $4.7x10^{-5}$	$5x10^{16}$	Good to excellent
PPS Polyphenylene Sulfide	Supec (GE) Ryton (Phillips)	$5.5x10^5$ – $2.9x10^6$	$1.4x10^4$ – $2.8x10^4$	260 - 350			Good to excellent
Polyethylene terephthalate	Mylar (Dupont)	$7.4x10^5$	$2.9x10^4$	~200	$3x10^{-5}$	10^{18}	Good to excellent
PI-5878G	HD Microsystems	$2x10^5$		~400	$2x10^{-5}$		Excellent
polyimide	Kapton (DuPont)	$3.7x10^5$	$3.35x10^4$	~400	$2x10^{-5}$	$1.5x10^{17}$	Excellent
Silicon		$2.9x10^7$	$1.45x10^5$	1410	$2.33x10^{-6}$		

2. BACKGROUND

Sensors that are used to detect IR radiation are confined to two classes; photon detectors and thermal detectors. Photon (quantum) detectors utilize devices that detect radiation by direct interaction of the radiation with the atomic lattice of the material. Thermal detectors, on the other hand, respond thermally to optical radiation, i.e. the detector's temperature depends on incident radiation [14]. A microbolometer is a thermal detector whose resistance depends on its temperature [15]. Biasing the detector with a constant DC current and measuring the output voltage determines the change of resistance caused by IR illumination. The relative change in the resistance magnitude with the change of temperature is an important figure of merit for microbolometers and is defined as the temperature coefficient of resistance,

$$TCR = \beta = \frac{1}{R}\frac{dR}{dT} \qquad (1)$$

where R is the electrical resistance and T is the temperature.

The voltage responsivity (R_v) of thermal detectors is defined as the output voltage by the incident light flux to the detector.

$$R_v = \frac{\eta \beta R I_b}{G_{th}\left(1 + \omega^2 \tau_{th}^2\right)^{1/2}} \qquad (2)$$

where η is the IR absorption coefficient of the sensing material, I_b is the bias current, G_{th} is the thermal conductance between the microbolometer and its surroundings, ω is the angular modulation frequency of the incident IR radiation, and τ_{th} is the thermal response time, defined as the ratio of the microbolometer's thermal capacitance to its thermal

Downloaded From: http://proceedings.spiedigitallibrary.org/ on 06/04/2013 Terms of Use: http://spiedl.org/terms

conductance. This shows that the responsivity is directly proportional to the TCR, and inversely proportional to the thermal conductance of the detector. Thus, a sensitive material of high TCR value is needed to achieve high responsivity, as well as good thermal isolation of this material and low thermal conductance to the heat sink. Semiconductor materials are used as sensitive materials because the magnitude of the TCR is typically much higher than that of a metal [16]. Micromachining techniques are applied to create a vacuum gap under the detector to provide low thermal conductance. Increasing the resistance value would increase the responsivity ($R_v \alpha R$). However, the Johnson voltage noise would also increase ($V_J \alpha R^{1/2}$) resulting in a signal-to-noise ratio increasing with the square root of the electrical resistance ($SNR \alpha R^{1/2}$). Increasing the bias current would increase the electrical power dissipated in the detector as well as the associated 1/f noise. A low thermal conductance on the other hand must be optimized with a low thermal mass so that the thermal time constant remains low. Another important figure of merit of microbolometers is the detectivity D^*, which provides an area normalized signal-to-noise ratio.

$$D^* = \frac{R_v \sqrt{A\Delta f}}{\Delta V_n} \tag{3}$$

where A is the effective area of the detector under radiation, $\Delta V_n / \sqrt{\Delta f}$ is the total noise voltage per unit root frequency bandwidth. Thus, higher responsivity values of a detector, as a result of a larger detector area or higher noise voltage, are considered in the detectivity.

An important figure of merit for a detector is its noise equivalent power (NEP), which is the input power necessary to give a unity signal-to-noise ratio [15,14].

$$NEP = \frac{\Delta V_n}{R_v} \tag{4}$$

The noise voltage, ΔV_n, includes the background noise produced by the radiative exchange with the surroundings, temperature fluctuation noise due thermal conductance to the heat sink, and the noise generated by the thermometer. The thermometer noise is made up of Johnson noise and 1/f-noise.

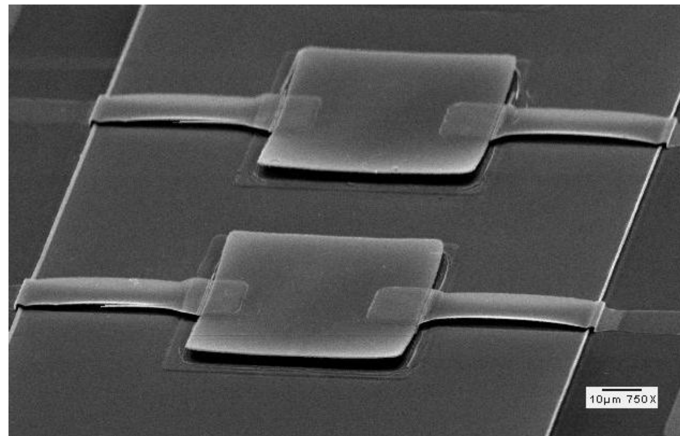

Fig 1: A SEM micrograph for a 60x60 µm^2 micromachined microbolometer on a flexible substrate. The sample was coated with 40 nm Au to eliminate charging of the polyimide by the SEM.

3. FABRICATION

The first attempt to fabricate microbolometers on flexible substrates was successfully accomplished in our laboratories. These detectors have undergone three generations. The first generation detectors on flexible substrates used commercial Kapton sheets bonded to Si wafer carriers. Those detectors achieved a responsivity of 2x10^3 V/W and a detectivity of 3x10^7 cmHz$^{1/2}$/W at 1µA of current [7]. In the second generation, we have used spun-coated polyimide films where the responsivity and detectivity peaked at 1.58x10^3 V/W and 4.91x10^6 cmHz$^{1/2}$/W respectively at 1 µA of current. The responsivity and detectivity in the third generation detectors that we present in this paper have been improved due to micromachining. An SEM micrograph of two microbolometers from one linear array is shown in Fig 1.

Downloaded From: http://proceedings.spiedigitallibrary.org/ on 06/04/2013 Terms of Use: http://spiedl.org/terms

The fabrication of devices on polyimide substrates requires careful consideration of the processing temperature. Low temperature processing is required such that the polyimide is not heated above the glass transition temperature at which the polyimide becomes liquid. In the case of PI-5878G, the glass transition temperature is 400 ^{0}C. Microbolometer square pixels were implemented on flexible substrates in linear 1x10 arrays, with different pixel area ranging from 40x40μm^2 to 80x80μm^2 using surface micromachining techniques. A schematic overview of the fabrication process is shown in Fig. 2. The device fabrication started with a <111> n-type 11.1-13.0 Ω-cm Si wafer. A turbo-pumped RF sputter system was used in all depositions at 10mTorr of pure Ar environment with 3-inch targets, separated from the substrate in a vertical, up-sputter assembly by 4 inches. A 400nm Si_3N_4 layer was sputtered at 200 Watts for adhesion and passivation of the polyimide layer. Five layers of PI-5878G were spun coated at 2000, 2100, 2200, 2300, 2400 and 2500rpm respectively. Each layer was soft-baked on a hot plate at 110^{0}C for 6 minutes before the application of the successive layer. The wafer was placed into an oven at room temperature and ramped up to 275^{0}C and cured for 5 hours. The combined layers formed a flexible polyimide substrate of ~ 40μm thick layer. Another 400nm Si_3N_4 layer was sputtered for polyimide passivation and to promote good adhesion between the polyimide and subsequent device layers.

a) Deposit Si_3N_4, spin coat PI-5878G, deposit Si_3N_4, deposit and pattern Al

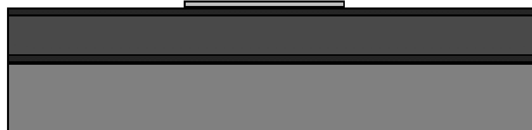

From bottom to top: Silicon Si_3N_4 (400nm) PI-5878G (40μm) Si_3N_4 (400nm) Al (260nm)

b) Spin coat PI2737 and pattern a mesa sacrificial layer

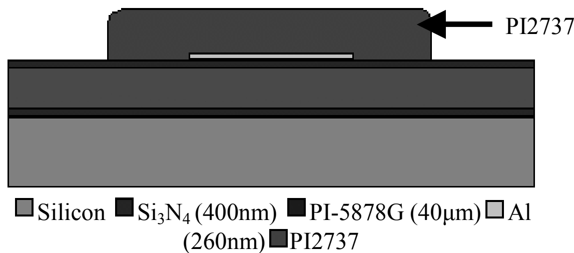

Silicon Si_3N_4 (400nm) PI-5878G (40μm) Al (260nm) PI2737

c) Pattern Au and Ti using lift off and wet etching

Silicon Si_3N_4 (400nm) PI-5878G (40μm) Al (260nm) PI2737 (1.88 μm) Ti (100nm) Au (70nm)

d) Deposit and pattern YBCO, ash sacrificial layer and separate from Si carrier

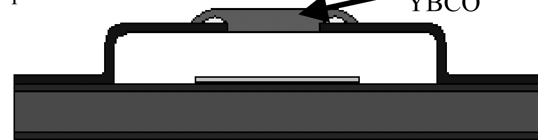

Si_3N_4 (400nm) PI-5878G (40μm) Al (260nm) PI2737 (1.88 μm) Ti (100nm) Au (70nm) YBCO (400nm)

Fig. 2: Simplified fabrication process flow for suspended microbolometers on a flexible substrate (not drawn to scale).

The nitride layer withstands most of the wet chemical etchants that we use in our fabrication procedure. A 70nm $SrTiO_3$ layer was sputtered at 100 W as a dry etch stop above the nitride layer. Al was then sputtered at 300W and patterned using S1813 photoresist and wet etching in a commercial aluminum etch solution for the formation of a 260nm Al micro-mirror in square patterns that are the same size as the YBCO thermometer (Fig. 2a). The photodefinable sacrificial polyimide (HD Microsystems PI2737) was spin coated at 2900rpm and sequentially soft baked for 60 seconds on hot plates at 65^{0}C and 95^{0}C. This layer was patterned by photolithography with a UV light exposure for 15 seconds and developed away using DI9040 developer and RI9180 rinse, resulting in a 1.88μm rectangular polyimide mesa structures extending 50μm around the pixel (Fig. 2b). Then, Ti electrode arms were patterned by liftoff using a 1.5-μm-thick negative photoresist (NR7-1500P). A 100nm Ti layer was then sputtered to form electrode arms between the YBCO thermistor and the bond pads. Ti was chosen because it has a low thermal conductance of 0.219W/cm-K to

Downloaded From: http://proceedings.spiedigitallibrary.org/ on 06/04/2013 Terms of Use: http://spiedl.org/terms

minimize the heat transfer from the pixel to the substrate and thereby attain a low thermal conductance parameter for high responsivity. Another 70nm of Au was sputtered at 100W over Ti to form contacts and bonding pads. Au forms a good electrical contact with YBCO and a good target for ultrasonic bonding. An ultrasonic agitator was used to lift off the Ti and Au films in an acetone bath. Since Au has higher thermal conductance (3.1W/cm-K) than Ti, Au was patterned on the electrode arms, using positive photolithography and wet etching with a $KI:I_2$ solution, to define the Au bond pads and Au electrical contacts to the YBCO thermistor (Fig. 2c). A 400nm YBCO layer was then sputtered at 90W power in 10 mTorr Ar from a single, composite 3-inch diameter $YBa_2Cu_3O_{6+x}$ target. YBCO has shown a relatively high TCR value of -3.1 % K^{-1} at room temperature. It can also be deposited by RF magnetron sputtering from a single composite target at room temperature without the need for post-deposition thermal treatment. The YBCO film was patterned using standard photolithography and wet etching with Al-etch. After patterning the YBCO, the detector was formed and the sacrificial polyimide layer (PI2737) was removed using O_2 plasma ashing with a Plasmaline asher at 120W RF power (Fig. 2d). Prior to removing the sacrificial layer, the wafer was divided into 6 pieces. Some of the pieces were ashed to suspend the microbolometer while others were tested with the sacrificial layer still in place. The ashing process required approximately 40 hours to complete. After ashing, the flexible polyimide substrate was removed from the silicon wafer carrier to produce IR microsensors on a flexible substrate (Fig. 3).

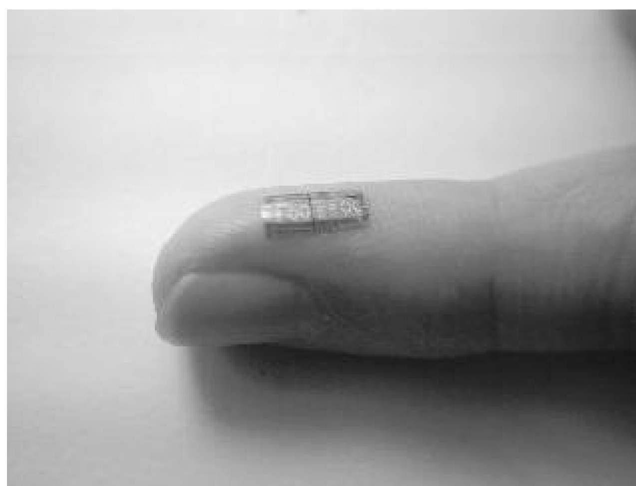

Fig 3: A flexible microbolometer “skin” on a finger. The 2 die shown contain 192 infrared microsensors.

4. RESULTS AND DISCUSSION

The performance of micromachined and non-micromachined microbolometers, before and after separation from silicon, was determined through optical and electrical characterization. The DC characteristics including noise, thermal conductance G, electrical resistance versus temperature, R-T, and TCR were measured at different temperatures on 40x40μm^2 microbolometers. The devices were packaged, ultrasonically bonded with Si-Al wires (1%Si) and mounted in a Leybold ROK 10-300K closed-cycle refrigerator, which was evacuated to ~100 mTorr. For the TCR measurement, a 1MΩ resistor was connected in series with the microbolometer to measure the current flowing through the microbolometer. Another 1MΩ resistor was shunted in parallel to both the series resistor and the microbolometer, to control the current flow at low temperatures and allow the voltage across the microbolometer to be measured indirectly. HP34401A multimeters were used to supply the current and measure the voltages to calculate the resistance and TCR values at different temperatures. A Lakeshore 91C temperature controller controlled the temperature of the refrigerator. The thermal conductance of the microbolometers was measured by resistive heating. The microbolometers were biased with various currents up to 2μA through an HP4142 DC source/monitor while keeping the substrate temperature constant. Changes in resistance that were purely due to Joule heating were used to calculate the thermal conductance G from the slope of the plotted resistance versus dissipated power.

$$R(T) = R_0 + \frac{1}{G}\frac{dR}{dT} I_b^2 R(T) \tag{7}$$

Downloaded From: http://proceedings.spiedigitallibrary.org/ on 06/04/2013 Terms of Use: http://spiedl.org/terms

Table II. Measured and fitted characteristics of the microbolometers on flexible substrates.

	DD1	DD6	DD10	DD12	DD13	DD15
Microbolometer Area (cm^2)	$36x10^{-6}$	$16x10^{-6}$	$16x10^{-6}$	$16x10^{-6}$	$16x10^{-6}$	$16x10^{-6}$
Micromachined	No	Yes	Yes	No	No	Yes
Separated from Si	No	No	No	Yes	Yes	Yes
Resistance (MΩ) at 290K	12.6	3.8	3.29	8.42	3.4	3.11
%TCR(K^{-1}) at 290K	-3.2	-	-3.4	-3.4	-	-
G_{th} (W/K) at 290K	$9.1x10^{-6}$	-	$4x10^{-7}$	$3.3x10^{-6}$	-	-
Max. Measured Responsivity (V/W) at 1μA	-	$3.2x10^4$ at 1μA	$3.9x10^4$ at 1μA	$1.1x10^4$ at 0.73μA	$4.7x10^3$ at 1μA	$6.1x10^4$ at 1μA
Max. Measured Detectivity ($cmHz^{1/2}/W$)	-	$4.2x10^7$ at 1μA	$1.1x10^8$ at 1μA	$8.5x10^6$ at 0.73μA	$1.8x10^7$ at 1μA	$1.2x10^8$ at 1μA
Thermal time constant τ_{th} (ms)	-	7.09	5.68	-	-	6.0
Thermal capacitance C (J/K)	-	-	$2.4x10^{-9}$	-	-	-
Absorption Coefficient, η	-	-	.29			-
NEP($W/Hz^{1/2}$)	-	$6.7x10^{-10}$	$3.0x10^{-10}$	$4.9x10^{-9}$	$1.0x10^{-9}$	$1.1x10^{-10}$

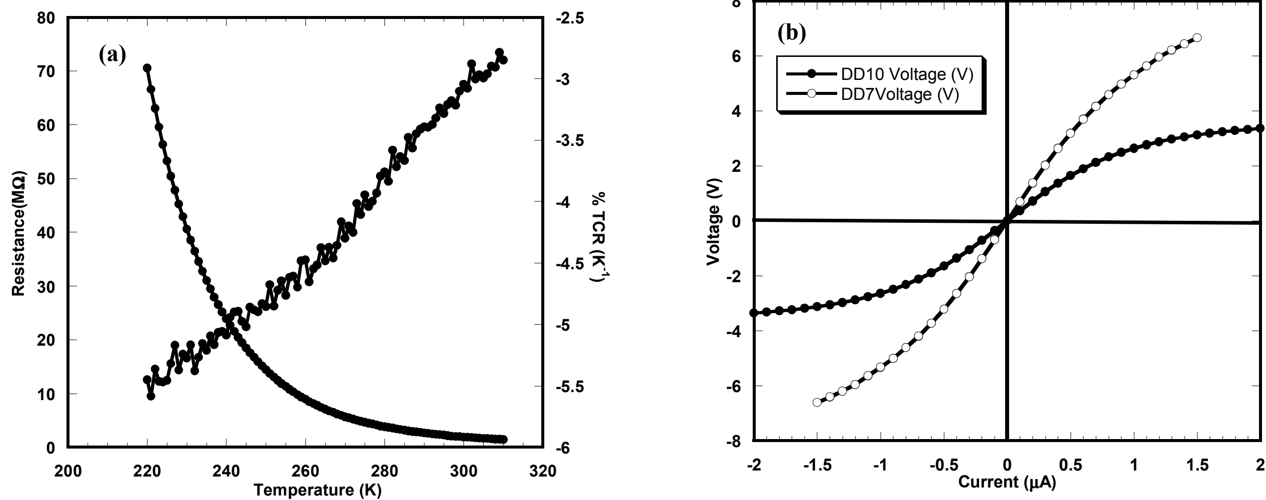

Fig 4: (a) Resistance and TCR versus temperature and (b) Current-voltage characteristics for devices DD7 and DD10

Device DD10 represents a micromachined microbolometer on a flexible substrate that was tested before separation from Si. Devices DD12 and DD15 are non-micromachined and micromachined bolometers on a flexible substrate after being separated from Si. The measured characteristics of these devices are summarized in Table II. The TCR of DD10 was -3.4 $\%K^{-1}$ and its G was $4.0x10^{-7}$ W/K at 290K. A device from an adjacent area of the wafer that was not micromachined showed a G of $9.1x10^{-6}$ W/K (DD1). This shows that removing the sacrificial layer and evacuating

Downloaded From: http://proceedings.spiedigitallibrary.org/ on 06/04/2013 Terms of Use: http://spiedl.org/terms

the underlying air under the microbolometer lowers the thermal conductance, which is necessary to achieve a high optical response from the detectors. However, no significant difference in the TCR was observed between the micromachined and non-micromachined devices. Fig 4 shows the electrical resistance R and TCR measurements versus temperature over the temperature range of 220K to 310K for DD10 at 100mTorr pressure. The I-V curves of DD10 and DD7 at 290K are also shown in Fig 4. Before micromachining, the devices displayed linear current-voltage (I-V) characteristics. At currents greater than 1μA, the micromachined detectors showed a slight non-linearity in the I-V characteristics resulting from Joule heating effects. These effects were noticed due to lower thermal conductance value resulting in less heat loss from the sensor to the substrate when biased with high currents. DD7 has higher thermal conductance ($G=7.8 \times 10^{-7}$W/K), and thus maintained a linear I-V curve.

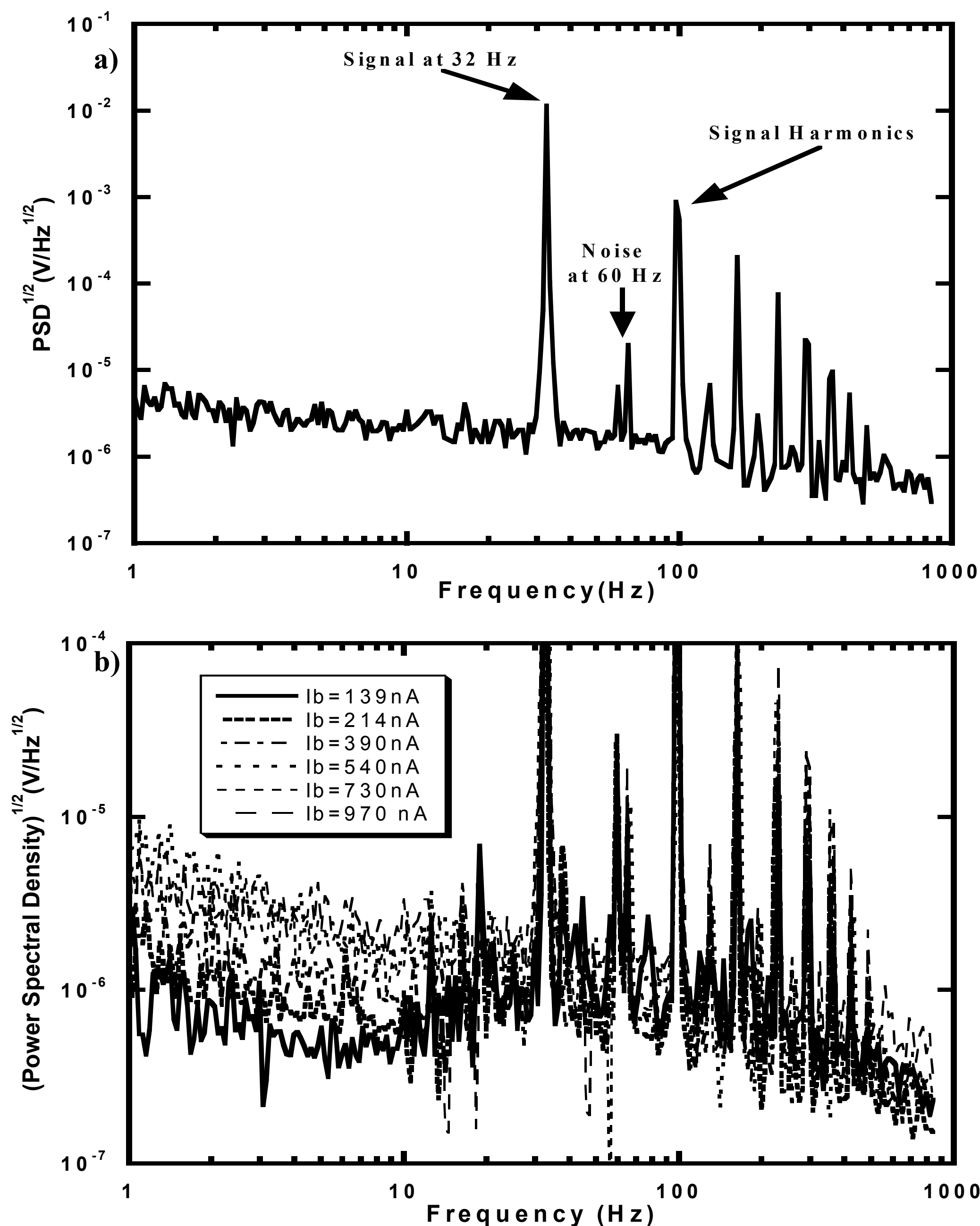

Fig 5: (a) Power spectral density with the signal at 32 Hz and 970nA of current bias and (b) Noise power spectral density at different bias currents.

Downloaded From: http://proceedings.spiedigitallibrary.org/ on 06/04/2013 Terms of Use: http://spiedl.org/terms

The optical characteristics were determined through illumination with broadband radiation from an Infrared Industries (manufacturer) thermal blackbody source controlled by a 101C temperature controller. The temperature of the source was kept constant at 990 ^{0}C throughout the measurements. The measurements were performed in-air and vacuum. In the in-air measurements, devices were illuminated with and without a ZnSe window to determine the transmission coefficient of the window for calibration for the vacuum measurements. A chopper was used to modulate the incident IR radiation while the bolometer was DC biased with different current values ranging from 319nA to 2.88μA with a battery powered low noise current source. The output voltage was amplified by a PAR113 preamplifier and measured with an HP 3562A dynamic signal analyzer. The responsivity was calibrated using an Oriel 70124 calibrated pyroelectric detector. The same setup was used to measure the optical response in vacuum where the detectors were mounted inside the cryostat that was evacuated to 70mTorr. The measurements were conducted inside a low-frequency noise shielded room.

Since the signal from the sensors is in the order of mV, the noise contributions are important in determining the sensor performance. The temperature of the substrate was not controlled throughout the optical characterization. Since the DC powered chopper has voltage fluctuations that are significant at low chopping frequencies, adding chopper noise to the total system noise, the noise measurement at a chopper frequency of 32 Hz was used to calculate the detectivity at optical modulation frequencies between 1 and 5.78 Hz. However, above this frequency, the actual electrical power spectral density was used at each chopper frequency. Fig. 5 shows the signal voltage output at 32Hz from DD10 at 1μA of bias current (Fig. 5a) as well as the noise spectrum at different current biases from 139nA to 970nA (Fig. 5b).

The responsivity was measured as a function of chopper frequency (Fig. 6a). The measured voltage responsivity and noise voltage, as noted above, were used to calculate the detectivity of the detector. The detectivity versus chopper frequency is plotted in Fig. 6b. Device DD10 has shown a responsivity of 3.9×10^4V/W at low frequencies, and a detectivity of 1.1×10^8 cmHz$^{1/2}$/W with 970nA of current bias. These results are comparable to those measured on microbolometers with a similar structure fabricated on Si substrates [9,10,12] and higher by an order of magnitude than those previously fabricated on flexible substrates without micromachining [7]. The decrease of thermal conductance with micromachining is responsible for the higher responsivity of this device compared to microbolometers that have not been micromachined. Fig 6b shows the responsivity detectivity measurements in air and in vacuum for device DD10. The output signal voltage, when measured in vacuum, has increased by a factor of 27 than that measured in air at low frequencies. This device has shown an NEP of 3×10^{-10} W/Hz$^{1/2}$. The cut off frequency was found by fitting the measured responsivity versus chopper frequency characteristic to Eq. (2). The thermal time constant was determined to be 5.68ms giving a thermal cut-off frequency of 28 Hz. The fitted low frequency responsivity, combined with the measured value of thermal conductance resulted in an absorption coefficient of 29% for this detector.

Device DD12, which was not micromachined, but was separated from silicon wafer carrier has shown a TCR value of -3.4 %K^{-1}. The thermal conductance for this device was measured to be 3.3×10^{-6} W/K. The responsivity and detectivity measurements performed in air through the ZnSe window showed a responsivity of 2.01×10^4 W/K at low frequencies and a detectivity of 1.05×10^7 cmHz$^{1/2}$/W with 970nA of current bias. Device DD15 was a micromachined sensor on a flexible substrate that was removed from the Si wafer carrier. This device was packaged by "soldering" the polyimide substrate to the package. As a result of this process, the polyimide substrate was slightly bent to be non-planar in the device package. The solder temperature is estimated to approached 350 ^{0}C during the mounting process yet no noticeable damage was caused to the sensor array. This device has shown the highest responsivity among the characterized detectors. Fig 7 shows the responsivity and detectivity measurements for this device, performed in vacuum. The low frequency responsivity was 6.1×10^4 V/W and the detectivity was 1.2×10^8 cmHz$^{1/2}$/W at 970nA of current bias.

5. CONCLUSION

A flexible polyimide skin containing microbolometer infrared sensors has been fabricated using conventional surface micromachining techniques with a polyimide sacrificial layer. No underlying bridge was used to support the detector. The fabrication process was fully CMOS compatible. The infrared microsensors have demonstrated responsivity close to 10^4 V/W and detectivity of 10^8 cmHz$^{1/2}$/W. Micromachining the devices has lowered the thermal conductance to 4.2×10^{-7} W/K and as a result enhanced the optical response by an order of magnitude over non-micromachined detectors. Currently, efforts are made to encapsulate the detectors in a vacuum cavity using a polyimide superstrate. The use of a superstrate will also protect the microbolometer arrays from damage by contact. Moreover, the

Downloaded From: http://proceedings.spiedigitallibrary.org/ on 06/04/2013 Terms of Use: http://spiedl.org/terms

combination of superstrate and substrate will enable the device plane to be a zero- or at least low-stress plane, thereby minimizing the mechanical strain on the infrared microsensors.

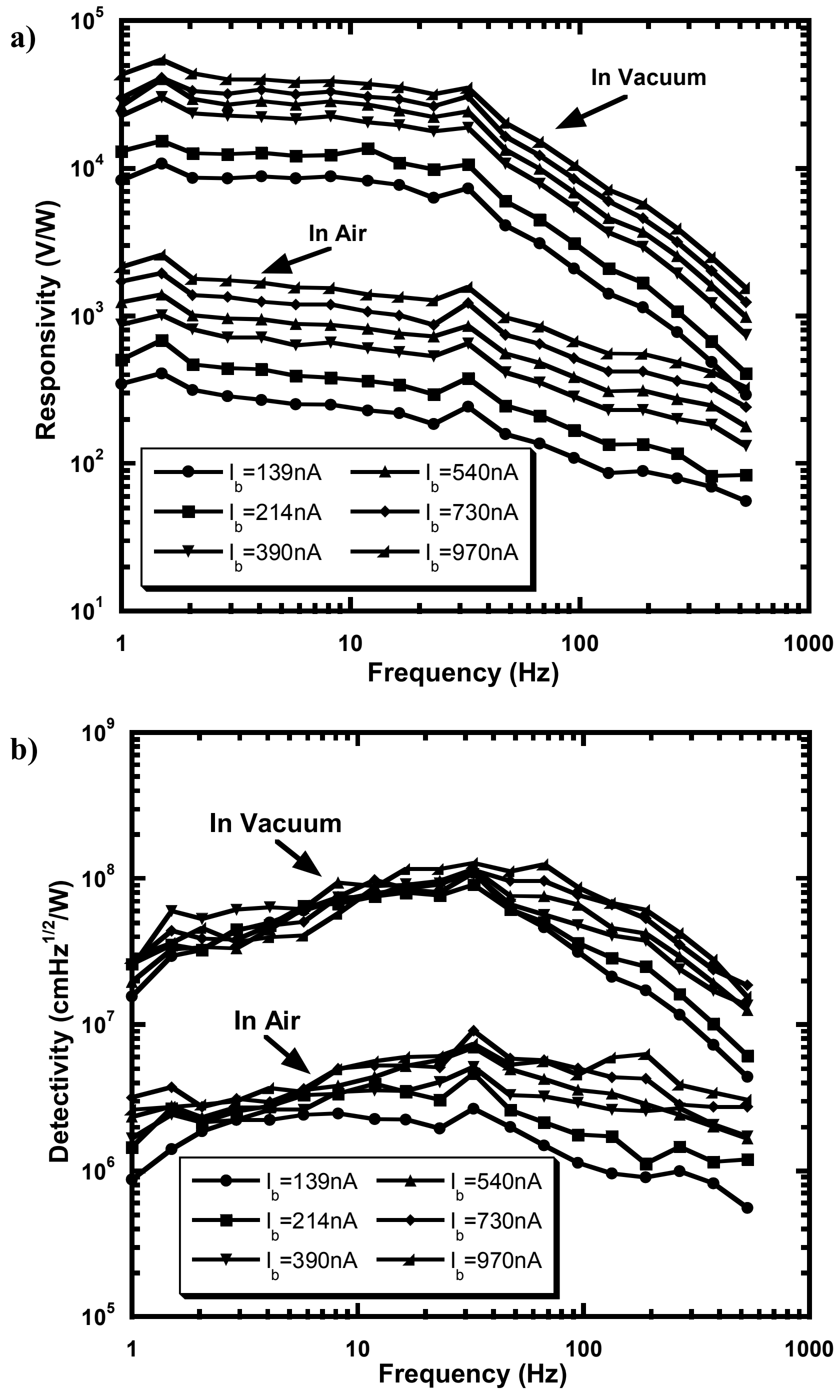

Fig 6: (a) Responsivity and (b) detectivity in air and in vacuum for device DD10.

Downloaded From: http://proceedings.spiedigitallibrary.org/ on 06/04/2013 Terms of Use: http://spiedl.org/terms

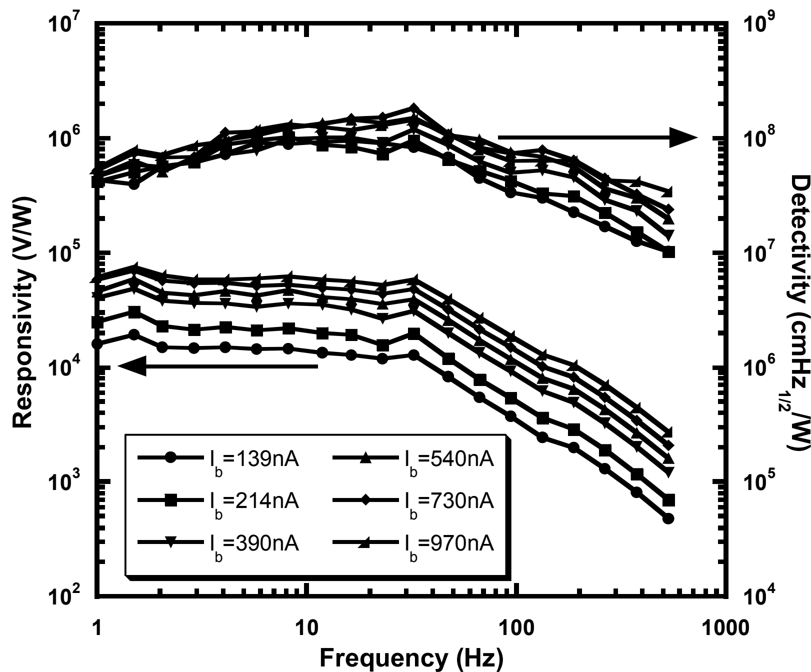

Fig 7: Responsivity and detectivity for device DD15 in vacuum.

6. ACKNOWLEDGMENTS

The authors would like to thank Ronald Elsenbaumer, Jim Florence, Nasir Basit, Guillaume Gbetibouo and Eduardo Maldonado for their help at the NanoFab Center at the University of Texas at Arlington. This work is based in part upon work supported by the NSF under grant ECS-0245612. The authors would like to thank the Cornell Nanofabrication Facility for fabricating the photolithography masks used in this investigation. Cornell Nano-Scale Science & Technology Facility (a member of the National Nanofabrication Users Network) is supported by the National Science Foundation under Grant ECS-9731293, its users, Cornell University and Industrial Affiliates.

REFERENCES

[1] Y. Lee, H. Li, S. J. Fonash, "Fabrication of high performance poly-Si thin film transistors on plastic*," NNUN Abstracts 2002*/Electronics, page 27.

[2] H. Klauk, D.J. Gundlach, J. A. Nichols, and T.N. Jackson, "Pentacene organic thin-film transistors for circuit and display applications," *IEEE Tran. on Electron Dev.* **ED-46**, 1258 (1999).

[3] F. Jiang, Y.-C. Tai, K. Walsh, T. Tsao, G.-B. Lee and C.-M. Ho, "A flexible MEMS technology and its first application to shear stress sensor skin," *Nagoya Castle*, Japan, pp. 465-470, 1997.

[4] Y. Xu, Y.-C. Tai, A. Huang, and C.-M. Ho, "IC-Integrated flexible shear-stress sensor skin", *Solid State Sensor, Actuator and Microsystems Workshop*, Hilton Head Island, South Carolina, June 2-6, 2002.

[5] D.J. Beebe and D.D. Denton, "A flexible polyimide-based package for silicon sensors," *Sensors and Actuators*, **A44**, 57 (1994).

[6] C. Bang and T. Pan, "Flexible heat flux sensor arrays," *AFOSR Contractor and Grantee Meeting on Turbulence and Internal Flows*, Atlanta, Georgia, 4-6 Sept. 1996.

[7] A. Yaradanakul, D. P. Butler and Z. Çelik-Butler, "Uncooled infrared microbolometers on a flexible substrate," *IEEE Tran. on Electron Dev.* , **49**, 930, (2002).

Downloaded From: http://proceedings.spiedigitallibrary.org/ on 06/04/2013 Terms of Use: http://spiedl.org/terms

[8] A. Yildiz, Z. Çelik-Butler, D. P. Butler, “Microbolometers in a flexible substrate for infrared detection,” accepted for publication in *IEEE Sensors Journal*.
[9] C. M. Travers, A. Jahanzeb, D. P. Butler, and Z. Çelik-Butler, “Fabrication of semiconducting YBaCuO surface-micromachined bolometer arrays„ *IEEE J. Microelectromechanical systems*, **6**, 271, 1997.
[10] A. Jahanzeb, C. M. Travers, Z. Çelik-Butler, D. P. Butler and S. G. Tan, “A semiconductor YBaCuO microbolometer for room temperature IR imaging,” *IEEE Tran. on Electron Dev.*, **44**, 1795, 1997.
[11] J.E. Gray, Z. Çelik-Butler, and D. P. Butler, “MgO sacrificial layer for micromachining uncooled Y-B-Cu-O IR microbolometers on Si_3N_4 bridges,” *IEEE J. Microelectromechanical Systems*, **8**, 192, (1999)
[12] M. Almasri, D. P. Butler, and Z. Çelik-Butler, “Self-supporting uncooled infrared microbolometers with low thermal mass,” *IEEE J. Microelectromechanical systems*, **10**, 469 (2001).
[13] http://www.hdmicrosystems.com .
[14] E. L. Dereniak, G. D. Boreman, *Infrared Detectors and Systems*, Chapter 8, John Wiley and Sons, 1996.
[15] P.W. Kruse, “A comparison of the limits to the performance of thermal and photon detector imaging arrays,” Infrared Phys. Technol. 36, 869, (1995).
[16] J. W. Gardner, *Microsensors Principles and Applications*, John Wiley and Sons, 1994.

Downloaded From: http://proceedings.spiedigitallibrary.org/ on 06/04/2013 Terms of Use: http://spiedl.org/terms